

# Pairing sizes in attractively interacting Fermi gases with Spin-orbit Couplings

Yu Yi-Xiang,<sup>1,2</sup> Jinwu Ye,<sup>2,3</sup> and Wu-Ming Liu<sup>1</sup>

<sup>1</sup>*Beijing National Laboratory for Condensed Matter Physics,*

*Institute of Physics, Chinese Academy of Sciences, Beijing 100190, China*

<sup>2</sup>*Department of Physics and Astronomy, Mississippi State University, MS, 39762, USA*

<sup>3</sup>*Key Laboratory of Terahertz Optoelectronics, Ministry of Education,  
Department of Physics, Capital Normal University, Beijing, 100048, China*

(Dated: July 27, 2018)

Extensive research has been lavished on effects of spin-orbit couplings (SOC) in attractively interacting Fermi systems in both neutral cold atom systems and condensed matter systems. Recently, it was suggested that a SOC drives a new class of BCS to BEC crossover which is different than the conventional one without a SOC. Here, we explore what are the most relevant physical quantities to describe such a new BCS to BEC crossover and their experimental detections. We extend the concepts of the pairing length and “Cooper-pair size” in the absence of SOC to Fermi systems with SOC. We investigate the dependence of chemical potential, pairing length, “Cooper-pair size” on the SOC strength and the scattering length at 3d (the bound state energy at 2d) for three attractively interacting Fermi gases with 3 dimensional (3d) Rashba, 3d Weyl and 2d Rashba SOC respectively. We show that only the pairing length can be used to characterize this new BCS to BEC crossover. Furthermore, it is the only length which can be directly measured by radio-frequency dissociation spectra type of experiments. We stress crucial differences among the pairing length, “Cooper-pair size” and the two-body bound state size. Our results provide the fundamental and global picture of the new BCS to BEC crossover and its experimental detections in various cold atom and condensed matter systems.

## I. INTRODUCTION

Spin-orbit coupling (SOC) has played important roles in various condensed matter systems such as anomalous Hall effects<sup>1</sup>, non-centrosymmetric superconductors with lifted spin degeneracy<sup>2</sup> and exciton superfluids in electron-hole semiconductor bilayers<sup>3,4</sup>. Recently the investigation and control of spin-orbit coupling (SOC) have become subjects of intensive research after the discovery of the topological insulators<sup>5,6</sup>. For example, the SOC is a critical determining factor leading to a whole new class of electronic states<sup>7</sup> such as various spin-orbital ordered states, spin liquids, various topological phases, etc. The 1D SOC which is a linear combination of Rashba and Dresselhauss SOC has been successfully generated in several experimental groups for neutral atoms both in Bose and Fermi gas<sup>8–11</sup>. Possible experimental constructions of 2D Rashba or Dresselhauss SOC and 3D Weyl SOC have also been proposed<sup>12,13</sup>. There are also extensive theoretical investigations on various important effects of SOC on attractively interacting<sup>14–17</sup> degenerate Fermi gases across BCS to BEC crossover. Collective excitations above the mean field states have also been calculated in<sup>18–21</sup>. The collective modes and magnetic transitions in repulsively interacting Fermi gas were investigated<sup>22,23</sup>. Recently, both staggered<sup>24</sup> and uniform<sup>25</sup> artificial magnetic fields have been generated in optical lattices. Scaling functions for various gauge-invariant and non-gauge invariant quantities across topological transitions driven by the SOC on an optical lattice have been derived<sup>26</sup>. Especially, it was also stressed in<sup>26</sup> that in contrast to condensed matter experiments where only gauge invariant quantities can be measured, both

gauge invariant and non-gauge invariant quantities can be measured by experimentally generating various non-Abelian gauges corresponding to the same set of Wilson loops. The interplay among the SOC, interactions and lattice geometries leading to new quantum phase, excitation spectrum and quantum phase transitions has also been explored<sup>27</sup>.

The BCS to BEC crossover is a long outstanding problem in both condensed matter<sup>28,29</sup> and cold atoms<sup>30</sup>. Conventional superconductors is well side the BCS limit, so mean field theory works well<sup>28,29</sup>. Due to its short coherence  $\xi$ , high temperature superconductors are near the BCS to BEC crossover, but still in the BCS side with well defined Fermi surface<sup>29,31</sup>, so quantum fluctuation effects are large. The BCS to BEC crossover of exciton superfluids in electron hole semiconductor bilayer can be tuned by the exciton density<sup>32–35</sup>. The BCS to BEC crossovers of attractively interacting neutral fermions are tuned by sweeping across a Feshbach resonance<sup>30</sup>. The effects of SOC on the BCS to BEC crossover has been investigated by several groups<sup>14–17</sup>. Especially, the authors in<sup>15</sup> found that when the SOC strength is well beyond the value of the topological Lifshitz transition of the non-interacting Fermi surfaces<sup>23,26</sup>, the overlap between the two-body wavefunction<sup>14,28</sup> and the “Cooper-pair wavefunction”<sup>36</sup> (see Sec. II-B for its definition) approaches to be 1. So they concluded that at a fixed scattering length at the BCS side (in the absence of SOC), the SOC drives a new BCS to BEC crossover which is in a different class than the one without a SOC driven by the exciton density<sup>32–35</sup> or Feshbach resonance<sup>30</sup>. However, as to be shown in this paper, the “Cooper-pair wavefunction” is useful for illustration purposes only instead of being physical, so its overlap with the two-body wavefunction is not phys-

ical, can not be measured experimentally. In order to describe the new BCS to BEC crossover driven by the SOC strength, it is important to identify and compute the most relevant physical quantity to describe such a new BCS to BEC crossover and then address its experimental detections.

In this paper, we address this outstanding problem by investigating 3 SOC coupled Fermi gases: (1) a 3D Fermi gas with a Rashba SOC (2) a 3D Fermi gas with a isotropic Weyl SOC (3) a 2D Fermi gas with a Rashba SOC. We first extend the concepts of the pairing length associated with a many-body wavefunction<sup>28,29,37</sup> and “Cooper-pair size”<sup>36</sup> associated with a “Cooper-pair wavefunction” in the absence of SOC to Fermi systems with a SOC. The three systems have different symmetries: the  $[U(1)_{spin} \times U(1)_{orbit}]_D$  symmetry at 3d where the  $D$  means the spontaneous rotation in spin and orbital space, the  $[SU(2)_{spin} \times SO(3)_{orbit}]_D$  symmetry at 3d and the  $[U(1)_{spin} \times U(1)_{orbit}]_D$  symmetry at 2d respectively. These symmetries determine the number of independent pairing lengths and Cooper-pair sizes to be 2, 1 and 1 respectively. We then study the dependence of chemical potential, pairing length, “Cooper-pair size” on the SOC strength  $\lambda$  for three attractively interacting Fermi gases. We show that from the BCS side at  $\lambda = 0$ , as the SOC strength increases, the chemical potential drops below the bottom of the single particle spectrum  $\mu_0 = -\frac{\lambda^2}{2m}$ , so it can be used to characterize qualitatively the BCS to BEC crossovers driven by the SOC strength. The pairing length decreases monotonically and quickly below the inter-particle spacing, so can be used to characterize quantitatively the BCS to BEC crossovers. Furthermore, the pairing length can be directly measured by using radio-frequency dissociation spectra type of experiments<sup>38</sup> as soon as the 2d and 3d SOC can be realized experimentally. In sharp contrasts, the “Cooper-pair size” used in the previous work<sup>14–16</sup> shows non-monotonic behaviors, so it may not be used to characterize the BCS to BEC crossover even qualitatively. Furthermore, it is not an experimentally measurable quantity. Starting from the BEC side at  $\lambda = 0$ , the effects of SOC are small, both the pairing length and the “Cooper-pair size” converge to the two-body bound state size<sup>14,28</sup>. We conclude that the pairing length is a much more robust concept than the “Cooper pair size”, it is also the only experimentally detectable physical quantity which can be used to describe the BCS to BEC crossover even quantitatively. We also discuss relations among the many-body BCS wavefunctions, the “Cooper-pair wavefunctions” and the two-body wavefunctions, therefore stress crucial differences among the pairing length, Cooper-pair size and the two body bound state size. The results provide a solid foundation for the fundamental physics of the new BCS to BEC crossover and its experimental detections. Our results should also shed considerable lights on condensed matter systems such as 2d exciton superfluids and 2d non-centrosymmetric superconductors.

The rest of the paper is organized as follows: In Sect. II, we first review the different definitions and concepts of pairing length and “Cooper pair size”, then extend their concepts to SOC system where the spin is not a conserved quantity. In Sect.III, for a 3d Rashba systems, we study how the chemical potential, the pairing length and the Cooper pair size change as the SOC strength increases, especially focus on their behaviors across the new BCS to BEC crossover driven by the SOC strength. To be complete, we also study how the the pairing length and the Cooper pair size change with the scattering lengths at fixed SOC strengths. We also discuss the crucial differences among the pairing length, Cooper-pair size and the two-body bound state size. In Sec.IV, we compute the same quantities on 3d Fermi gas with an isotropic Weyl SOC. In Sec.V, we perform similar calculations on 2d Fermi gas with Rashba SOC which needs a different regularization than the two 3d systems discussed in the previous two sections. In Sec.VI, we discuss the implications of the results achieved in the previous sections, especially in the Sec. V, on several condensed matter systems. We summarize the main results and discuss several exciting perspectives in Sec. VII.

## II. EXTEND PARING LENGTH AND COOPER PAIR SIZE TO SOC SYSTEMS

We consider a homogeneous Fermi gas with an attractive contact potential:

$$H = \sum_{\mathbf{p}, \sigma=\uparrow, \downarrow} c_{\mathbf{p}\sigma}^\dagger \left( \frac{\mathbf{p}^2}{2m} - \mu \right) c_{\mathbf{p}\sigma} + V_{soc} + \frac{g}{V} \sum_{\mathbf{p}, \mathbf{q}, \mathbf{s}} c_{\frac{\mathbf{s}}{2} + \mathbf{p}\uparrow}^\dagger c_{\frac{\mathbf{s}}{2} - \mathbf{p}\downarrow}^\dagger c_{\frac{\mathbf{s}}{2} - \mathbf{q}\downarrow} c_{\frac{\mathbf{s}}{2} + \mathbf{q}\uparrow}, \quad (1)$$

where  $d = 2, 3$ , and  $V_{soc}$  is the spin-orbit coupling (SOC) term which can be Rashba or Dresselhauss type or 3d Weyl isotropic SOC.

It was known that the interaction  $g$  need to be regularized differently in 2d and 3d. In 3d, the  $g$  can be regularized by the s-wave scattering length  $a_s$ :  $\frac{1}{g} = \frac{m}{4\pi\hbar^2 a_s} - \frac{1}{V} \sum_{\mathbf{p}} \frac{1}{2\epsilon_{\mathbf{p}}}$  where  $V$  is the volume of the system and  $\epsilon_{\mathbf{p}} = \frac{\mathbf{p}^2}{2m}$  is the free particle dispersion. In 2d, the  $g$  can be regularized by the two-body binding energy  $\epsilon_B$ :  $\frac{1}{g} = -\frac{1}{V} \sum_{\mathbf{p}} \frac{1}{2\epsilon_{\mathbf{p}} + \epsilon_B}$ .

By introducing the order parameter  $\Delta = \frac{g}{V} \sum_{\mathbf{p}} \langle c_{-\mathbf{p}\downarrow} c_{\mathbf{p}\uparrow} \rangle$ , one can reduce the interaction term to the mean-field form:  $H_{int}^{MF} = \sum_{\mathbf{p}} \left( \Delta^* c_{-\mathbf{p}\downarrow} c_{\mathbf{p}\uparrow} + \Delta c_{\mathbf{p}\uparrow}^\dagger c_{-\mathbf{p}\downarrow}^\dagger \right) - \frac{V|\Delta|^2}{g}$ . The chemical potential  $\mu$  and the order parameter  $\Delta$  can be determined by two self-consistent equations—the number equation:  $n = \frac{1}{V} \sum_{\mathbf{p}, \sigma} \langle c_{\mathbf{p}\sigma}^\dagger c_{\mathbf{p}\sigma} \rangle_{MF}$  and the gap equation:  $\Delta = \frac{g}{V} \sum_{\mathbf{p}} \langle c_{-\mathbf{p}\downarrow} c_{\mathbf{p}\uparrow} \rangle_{MF}$ .

Without SOC, the pairing length has been calculated in Fermi gas across the whole BCS to BEC crossover tuned by Feshbach resonance in<sup>37</sup>. Most importantly, it has been measured in MIT's group lead by Ketterle using radio-frequency dissociation spectra throughout the whole BCS to BEC crossover in<sup>38</sup>. However, the effects of SOC on the pairing correlation lengths have never been studied so far. In this section, we first review the definition and concepts of the pairing length without SOC, then extend to the SOC case.

### A. Pairing length

For a spin singlet superfluid without SOC, the fermion pair correlation functions are defined as:

$$\psi(\vec{r}) = \frac{1}{n^2} \langle c_{\uparrow}^{\dagger}(\vec{r}) c_{\downarrow}^{\dagger}(0) c_{\downarrow}(0) c_{\uparrow}(\vec{r}) \rangle - \frac{1}{4}, \quad (2)$$

where  $n$  is the particle density and the average is taken with respect to the BCS ground state  $|\Phi\rangle = |BCS\rangle$  (in second quantized form):

$$\begin{aligned} |\Phi\rangle &= \Pi_{\vec{k}} (u_{\vec{k}} + v_{\vec{k}} c_{\vec{k}\uparrow}^{\dagger} c_{-\vec{k}\downarrow}^{\dagger}) |0\rangle \\ &= (\Pi_{\vec{k}} u_{\vec{k}}) \Pi_{\vec{k}} (1 + \frac{v_{\vec{k}}}{u_{\vec{k}}} c_{\vec{k}\uparrow}^{\dagger} c_{-\vec{k}\downarrow}^{\dagger}) |0\rangle \\ &= (\Pi_{\vec{k}} u_{\vec{k}}) \exp[\sum_{\vec{k}} \frac{v_{\vec{k}}}{u_{\vec{k}}} c_{\vec{k}\uparrow}^{\dagger} c_{-\vec{k}\downarrow}^{\dagger}] |0\rangle, \end{aligned} \quad (3)$$

which obviously hosts in-definite number of electrons. Its first quantized form was discussed in<sup>28</sup>.

The pairing length is defined as<sup>37,38</sup>

$$\xi_{pair}^2 = \frac{\int d\vec{r} \psi(\vec{r}) r^2}{\int d\vec{r} \psi(\vec{r})}. \quad (4)$$

At the mean field level, Eqn.2 reduces to:

$$\psi(\vec{r}) = \frac{1}{n^2} |\langle \Phi | c_{\uparrow}^{\dagger}(\vec{r}) c_{\downarrow}^{\dagger}(0) | \Phi \rangle|^2, \quad (5)$$

where  $|\Phi\rangle = |BCS\rangle$ .

Under the mean field approximation, Eqn.4 can be rewritten as<sup>38</sup>:

$$\xi_{pair}^2 = \frac{\langle \psi_{\alpha\beta} | r^2 | \psi_{\alpha\beta} \rangle}{\langle \psi_{\alpha\beta} | \psi_{\alpha\beta} \rangle}, \quad (6)$$

where  $\psi_{\alpha\beta}(\vec{r}) = \langle \Phi | c_{\alpha}^{\dagger}(\vec{r}) c_{\beta}^{\dagger}(0) | \Phi \rangle$  with  $\alpha = \uparrow, \beta = \downarrow$ .

The Fourier transform of Eqn.6 to  $\vec{k}$  space leads to:

$$\xi_{pair}^2 = \frac{\langle \psi_{\alpha\beta} | \nabla_{\vec{k}}^2 | \psi_{\alpha\beta} \rangle}{\langle \psi_{\alpha\beta} | \psi_{\alpha\beta} \rangle}, \quad \alpha = \uparrow, \beta = \downarrow, \quad (7)$$

where  $\psi_{\alpha\beta}(\vec{k}) = \langle \Phi | c_{\alpha}^{\dagger}(\vec{k}) c_{\beta}^{\dagger}(-\vec{k}) | \Phi \rangle$  is the Fourier transform of  $\psi_{\alpha\beta}(\vec{r})$  with  $\alpha = \uparrow, \beta = \downarrow$ . More straightforwardly, Eqn.6 in real space and Eqn.7 in momentum space are Fourier transform to each other.

For a BEC to BCS crossover without SOC, the only pairing is the singlet pairing so  $\psi_{\uparrow\downarrow}(\vec{k}) = \langle \Phi | c_{\uparrow}^{\dagger}(\vec{k}) c_{\downarrow}^{\dagger}(-\vec{k}) | \Phi \rangle = u_{\vec{k}} v_{\vec{k}} = \frac{\Delta_0}{2E_{\vec{k}}}$  which is given and shown in Fig.3 in<sup>37</sup>.

It is important to point out that Eqn.2 and Eqn.4 hold in general, while Eqn.5 and 6 hold only at the mean field level. Only at the mean field level, one can “intuitively” interpret Eqn.5 and 6 as the expectation value of  $r^2$  over the “pairing wavefunction”  $\psi_{\alpha\beta}(\vec{r}) = \langle \Phi | c_{\alpha}^{\dagger}(\vec{r}) c_{\beta}^{\dagger}(0) | \Phi \rangle$  with  $\alpha = \uparrow, \beta = \downarrow$ . Although the concept of pairing length Eqn.4 hold in general, such a wavefunction interpretation breaks down beyond the mean field.

In the presence of SOC, due to the non-conservation of spins, one need to average over all the spin components to define the fermion pair correlation functions, so Eqn.2 should be replaced by

$$\psi(\vec{r}) = \frac{1}{n^2} \sum_{\alpha, \beta} \langle c_{\alpha}^{\dagger}(\vec{r}) c_{\beta}^{\dagger}(0) c_{\beta}(0) c_{\alpha}(\vec{r}) \rangle - 1, \quad (8)$$

where  $n$  is the particle density. Eqn.4 remains.

At mean field level, following the steps to derive Eqns.5 and 6 leads to the pairing length in the presence of SOC:

$$\xi_i^2 = \frac{\sum_{\vec{k}, \alpha, \beta} \langle \psi_{\alpha\beta} | \partial_{k_i}^2 | \psi_{\alpha\beta} \rangle}{\sum_{\vec{k}, \alpha, \beta} \langle \psi_{\alpha\beta} | \psi_{\alpha\beta} \rangle}, \quad \alpha, \beta = \uparrow, \downarrow, \quad (9)$$

which could be measured by radio-frequency dissociation spectra used in the experiment<sup>38</sup> in the presence of SOC. After the spin sum, the orbital symmetry of the  $U(1)_{orbit}, O(3)_{orbit}, U(1)_{orbit}$  of the three systems to be discussed in the following three sections will be recovered. However, one still need to distinguish the pairing correlation length within  $xy$  plane and along  $z$  direction  $\xi_{xy}^2 \neq \xi_z^2$  in the first and the third system.

### B. “Cooper pair size”

In fact, one can also define the “Cooper-pair size” through the “Cooper pair wavefunction”<sup>28,39</sup>. Removing the exponential in the normalized BCS wave function without SOC in Eqn.3 leads to the singlet “Cooper-pair wavefunction” in second quantized form:

$$|g_{cp}\rangle = \sum_{\vec{k}} \frac{v_{\vec{k}}}{u_{\vec{k}}} c_{\vec{k}\uparrow}^{\dagger} c_{-\vec{k}\downarrow}^{\dagger} |0\rangle, \quad (10)$$

which hosts only two paired electrons. It can be understood as the two electron components of the many-body wavefunction.

One can extract the “Cooper-pair wavefunction” in the real space in the first quantization:

$$g_{cp}(\vec{r}) = g_{\uparrow\downarrow}(\vec{r}) (|\uparrow\downarrow\rangle - |\downarrow\uparrow\rangle), \quad g_{\uparrow\downarrow}(\vec{r}) = \sum_{\vec{k}} e^{i\vec{k}\cdot\vec{r}} \frac{v_{\vec{k}}}{u_{\vec{k}}}. \quad (11)$$

It is necessary to point out that this “Cooper-pair wavefunction” is different than the original pairing problem of two electrons near a Fermi surface first achieved by Cooper by solving the Schrodinger equation<sup>28</sup>.

The “Cooper pair size”<sup>36</sup> is defined by<sup>28,39</sup>

$$l_{pair}^2 = \frac{\int d\vec{r} |g_{\uparrow\downarrow}(\vec{r})|^2 r^2}{\int d\vec{r} |g_{\uparrow\downarrow}(\vec{r})|^2} = \frac{\langle g_{cp} | r^2 | g_{cp} \rangle}{\langle g_{cp} | g_{cp} \rangle}. \quad (12)$$

The Fourier transform of Eqn.12 to  $\vec{k}$  space leads to:

$$l_{pair}^2 = \frac{\langle g_{\alpha\beta} | \nabla_{\vec{k}}^2 | g_{\alpha\beta} \rangle}{\langle g_{\alpha\beta} | g_{\alpha\beta} \rangle}, \quad \alpha = \uparrow, \beta = \downarrow, \quad (13)$$

where  $g_{\uparrow\downarrow}(\vec{k}) = \frac{v_{\vec{k}}}{u_{\vec{k}}}$  is the Fourier transform of  $g_{\uparrow\downarrow}(\vec{r})$ . This should be contrasted with  $\psi_{\uparrow\downarrow}(\vec{k}) = \langle \Phi | c_{\uparrow}^\dagger(\vec{k}) c_{\downarrow}^\dagger(-\vec{k}) | \Phi \rangle = u_{\vec{k}} v_{\vec{k}} = \frac{\Delta_0}{2E_{\vec{k}}}$  used in Eqn.7.

It is important to point out that Eqn.3,11,12,13 hold only in mean field level. Only at the mean field level, one can “intuitively” interpret Eqn.12 and 13 as the expectation value of  $r^2$  over the “Cooper-pair wavefunction” Eqn.11. However, the concept of Cooper-pair size Eqn.13 breaks down beyond the mean field theory.

In the presence of SOC, after writing the mean field ground state in the form  $|BCS\rangle_{SOC} \propto \exp[\sum_{\vec{k}} g_{\alpha\beta}(\vec{k}) c_{\vec{k}\alpha}^\dagger c_{-\vec{k}\beta}^\dagger] |0\rangle$ , then one can extract the Cooper pair size<sup>28,39</sup> as

$$l_i^2 = \frac{\sum_{\vec{k}, \alpha, \beta} \langle g_{\alpha\beta} | \partial_{k_i}^2 | g_{\alpha\beta} \rangle}{\sum_{\vec{k}, \alpha, \beta} \langle g_{\alpha\beta} | g_{\alpha\beta} \rangle}, \quad \alpha, \beta = \uparrow, \downarrow, \quad (14)$$

where the average over all the spin components is performed. Note that  $g_{\alpha\beta}(\vec{k})$  is very much different than  $\phi_{\alpha\beta}(\vec{k})$ , so we may expect quite different behaviors from the two lengths. These will be explicitly demonstrated in the following sections. It is the pairing length which is measured in the MIT experiment<sup>38</sup>.

In the following, we apply the formalism to the 3d Rashba SOC, 3d Weyl SOC and 2d Rashba SOC systems.

### III. 3D FERMION GAS WITH A RASHBA SOC

The 3d Rashba SOC can be written as

$$V_{3d-ra} = \frac{\lambda}{m} \sum_{\vec{p}} p_{\perp} \left[ e^{-i\varphi_{\vec{p}}} c_{\vec{p}\uparrow}^\dagger c_{\vec{p}\downarrow} + e^{i\varphi_{\vec{p}}} c_{\vec{p}\downarrow}^\dagger c_{\vec{p}\uparrow} \right], \quad (15)$$

where  $\lambda$  is the SOC strength,  $p_{\perp} = \sqrt{p_x^2 + p_y^2}$  and  $\varphi_{\vec{p}} = \text{Arg}(p_x + ip_y)$ . This model has been studied by previous works<sup>16,17</sup> with different focuses. The single particle part  $H_0$  in the Hamiltonian Eq. 1 can be diagonalized in the helicity base as

$$H_0 = \sum_{\vec{p}} \left( \xi_{\vec{p}+} h_{\vec{p}+}^\dagger h_{\vec{p}+} + \xi_{\vec{p}-} h_{\vec{p}-}^\dagger h_{\vec{p}-} \right), \quad (16)$$

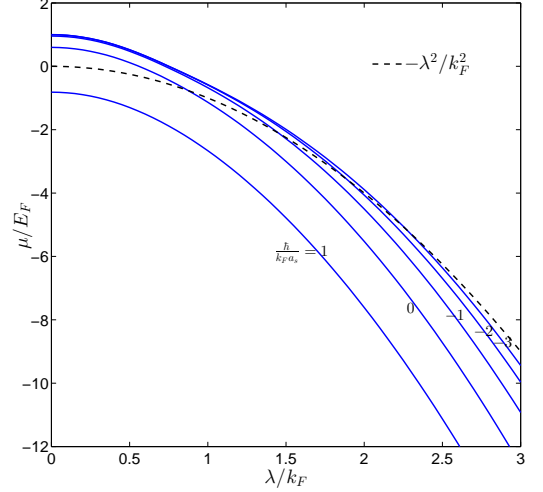


FIG. 1. The chemical potential  $\mu$  versus  $\lambda$  in a 3D Rashba SOC for different scattering lengths. The dashed line is the bottom of the single particle spectrum  $\mu_0 = -\frac{\lambda^2}{2m}$ . Starting from the BCS side at  $\lambda = 0$ , as  $\lambda$  increases, the  $\mu$  drops below  $\mu_0$ . This fact indicates that the system evolves into the BEC state.

where  $\xi_{\vec{p}\pm} = \frac{p_{\perp}^2}{2m} \pm \frac{\lambda p_{\perp}}{m} - \mu$  and the two helicity operators are:

$$\begin{aligned} h_{\vec{p}+} &= [c_{\vec{p}\uparrow} + e^{-i\varphi_{\vec{p}}} c_{\vec{p}\downarrow}] / \sqrt{2}, \\ h_{\vec{p}-} &= [e^{i\varphi_{\vec{p}}} c_{\vec{p}\uparrow} - c_{\vec{p}\downarrow}] / \sqrt{2}. \end{aligned} \quad (17)$$

In the helicity base, the mean-field interaction can be rewritten as  $H_{int}^{MF} = -\frac{1}{2} \sum_{\vec{p}} \left( \Delta_0 e^{-i\varphi_{\vec{p}}} h_{\vec{p}+}^\dagger h_{-\vec{p}+}^\dagger + \Delta_0 e^{i\varphi_{\vec{p}}} h_{\vec{p}-}^\dagger h_{-\vec{p}-}^\dagger + h.c. \right) - \frac{V|\Delta|^2}{g}$ . The total Hamiltonian  $H = H_0 + H_{int}^{MF}$  can be diagonalized by a Bogoliubov transformation:

$$\begin{aligned} H &= \sum_{\vec{p}} \left( E_{\vec{p}+} \alpha_{\vec{p}+}^\dagger \alpha_{\vec{p}+} + E_{\vec{p}-} \alpha_{\vec{p}-}^\dagger \alpha_{\vec{p}-} \right) \\ &\quad - \sum_{\vec{p}} \frac{E_{\vec{p}+} + E_{\vec{p}-}}{2} - \frac{V|\Delta_0|^2}{g}, \end{aligned} \quad (18)$$

where the quasiparticle excitation energy  $E_{\vec{p}\pm} = \sqrt{\xi_{\vec{p}\pm}^2 + |\Delta_0|^2}$ , and the quasi-particle operators:

$$\begin{aligned} \alpha_{\vec{p}+} &= \sqrt{\frac{E_{\vec{p}+} + \xi_{\vec{p}+}}{2E_{\vec{p}+}}} e^{i\varphi_{\vec{p}}} h_{\vec{p}+} - \sqrt{\frac{E_{\vec{p}+} - \xi_{\vec{p}+}}{2E_{\vec{p}+}}} h_{-\vec{p}+}^\dagger, \\ \alpha_{\vec{p}-} &= \sqrt{\frac{E_{\vec{p}-} + \xi_{\vec{p}-}}{2E_{\vec{p}-}}} e^{-i\varphi_{\vec{p}}} h_{\vec{p}-} - \sqrt{\frac{E_{\vec{p}-} - \xi_{\vec{p}-}}{2E_{\vec{p}-}}} h_{-\vec{p}-}^\dagger, \end{aligned} \quad (19)$$

where all anticommutation relations hold ( $\{\alpha_{\vec{p}+}, \alpha_{\vec{p}+}^\dagger\} = 1$ ,  $\{\alpha_{\vec{p}+}, \alpha_{\vec{p}-}^\dagger\} = 0$ , and so on).

At zero temperature, the two self-consistent equations become

$$n = \frac{1}{V} \sum_{\mathbf{p}} \left[ 1 - \frac{\xi_{\mathbf{p}+}}{2E_{\mathbf{p}+}} - \frac{\xi_{\mathbf{p}-}}{2E_{\mathbf{p}-}} \right],$$

$$\frac{1}{g} = -\frac{1}{4V} \sum_{\mathbf{p}} \left[ \frac{1}{E_{\mathbf{p}+}} + \frac{1}{E_{\mathbf{p}-}} \right], \quad (20)$$

where, as said in the Sec.II, the interaction strength  $g$  can be regularized by the s-wave scattering length  $a_s$ :  $\frac{1}{g} = \frac{m}{4\pi\hbar^2 a_s} - \frac{1}{V} \sum_{\mathbf{p}} \frac{1}{2\epsilon_{\mathbf{p}}}$ . In the rest of the section, we will determine the chemical potential  $\mu$ , the pairing length  $\xi_i$  in Eqn.9, the Cooper pair size  $l_i$  in Eqn.14. Finally we will compare our many body results with the corresponding two-body results<sup>14</sup>.

### A. Chemical potential across BCS to BEC crossover

One can find the chemical potential  $\mu$  by solving Eqn.20. It is shown in Fig.1. As a contrast, the minimum of the single-particle excitation energy  $\mu_0 = \text{Min}_{\mathbf{p}} \{ \frac{p^2}{2m} - \frac{\lambda p_{\perp}}{m} \} = -\frac{\lambda^2}{2m}$  is also plotted in Fig.1. We can qualitatively assign the region with  $\mu > \mu_0$  as the BCS region and  $\mu < \mu_0$  as the BEC region. As shown in Fig.1, starting from the BCS side at  $\lambda = 0$ , as  $\lambda$  increases, the  $\mu$  drops below  $\mu_0$ . Therefore, we conclude that Rashba SOC can drive a crossover from BCS to BEC as first pointed out in<sup>15</sup>.

### B. Pairing length across BCS to BEC crossover

The BCS ground state can be written as:

$$|BCS\rangle = \prod_{\mathbf{p}}' \alpha_{\mathbf{p}+} \alpha_{-\mathbf{p}+} \alpha_{\mathbf{p}-} \alpha_{-\mathbf{p}-} |0\rangle$$

$$\propto \exp \sum_{\mathbf{p}}' \left[ w_{\mathbf{p}+} e^{-i\varphi_{\mathbf{p}}} h_{\mathbf{p}+}^{\dagger} h_{-\mathbf{p}+}^{\dagger} + w_{\mathbf{p}-} e^{i\varphi_{\mathbf{p}}} h_{\mathbf{p}-}^{\dagger} h_{-\mathbf{p}-}^{\dagger} \right] |\mathbf{0}\rangle$$

where the  $\prime$  means half of the momentum space and  $|0\rangle$  is the electron vacuum state and  $w_{\mathbf{p}\pm} = \sqrt{\frac{E_{\mathbf{p}\pm} - \xi_{\mathbf{p}\pm}}{E_{\mathbf{p}\pm} + \xi_{\mathbf{p}\pm}}}$ .

From Eqn.21, one can find the singlet pairing amplitude:

$$\psi_{\uparrow\downarrow}(\mathbf{p}) = \frac{\langle BCS | c_{\mathbf{p}\uparrow}^{\dagger} c_{-\mathbf{p}\downarrow}^{\dagger} | BCS \rangle}{\langle BCS | BCS \rangle} \quad (22)$$

$$= -\frac{1}{2} \left( \frac{w_{\mathbf{p}+}}{1 + w_{\mathbf{p}+}^2} + \frac{w_{\mathbf{p}-}}{1 + w_{\mathbf{p}-}^2} \right)$$

$$= -\frac{\Delta_0}{4} \sum_{\alpha=\pm} 1/E_{\mathbf{p},\alpha}$$

$$= -\psi_{\downarrow\uparrow}(-\mathbf{p}) = -\psi_{\downarrow\uparrow}(\mathbf{p}), \quad (23)$$

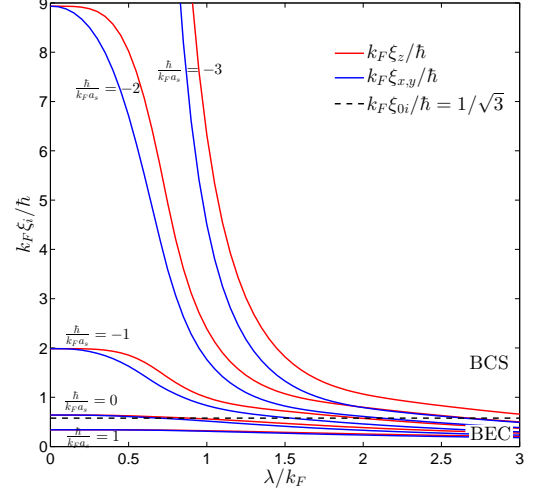


FIG. 2. The pairing length defined in Eqn.9 along  $x$  direction (red lines) ( $\xi_x = \xi_y$ ) and along the  $z$  (blue lines) direction as a functions of 3d Rashba SOC strength  $\lambda$ . The dashed line is a guidance line where  $k_F \xi_0 = \hbar$  ( $k_F \xi_{0i} = \hbar/\sqrt{3}$  for each component). Starting from the BCS side at  $\lambda = 0$ , it decreases monotonically and quickly below the reference line, so describe precisely the new BCS to BEC crossover driven by the SOC strength. Starting from the BEC side at  $\lambda = 0$ , the effects of SOC are small.

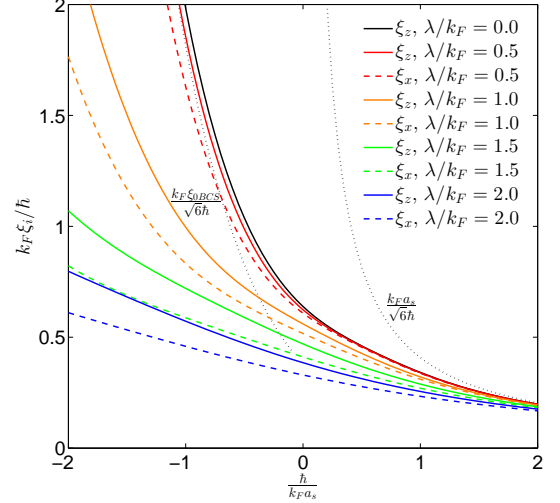


FIG. 3. The pairing lengths  $\xi_z > \xi_x = \xi_y$  at a fixed 3d Rashba SOC strength versus the scattering length. Different colors stand for different SOC strengths. Solid (dashed) lines stand for  $\xi_z$  ( $\xi_x = \xi_y$ ). The dark dotted line on the left (right) is its BCS (BEC) limit  $\frac{1}{\sqrt{6}} k_F \xi_{0BCS} = \frac{1}{8\sqrt{6}e^2} e^{-\frac{\pi\hbar}{2k_F a_s}} (\frac{k_F a_s}{\sqrt{6}})$  at  $\lambda = 0$ . On the BCS side, the SOC effects are dramatic, but on the BEC side, the SOC effects are small, all curves converge to the right dotted line  $\frac{k_F a_s}{\sqrt{6}}$  from below.

and the triplet pairing amplitude:

$$\begin{aligned}
\psi_{\uparrow\uparrow}(\mathbf{p}) &= \frac{\langle BCS | c_{\mathbf{p}\uparrow}^\dagger c_{-\mathbf{p}\uparrow}^\dagger | BCS \rangle}{\langle BCS | BCS \rangle} \\
&= \frac{1}{2} \left( \frac{w_{\mathbf{p}+}}{1 + w_{\mathbf{p}+}^2} - \frac{w_{\mathbf{p}-}}{1 + w_{\mathbf{p}-}^2} \right) e^{i\varphi_{\mathbf{p}}} \\
&= -\frac{\Delta_0}{4} e^{i\varphi_{\mathbf{p}}} \sum_{\alpha=\pm} \alpha / E_{\mathbf{p},\alpha} \\
&= -\psi_{\downarrow\downarrow}^*(\mathbf{p}). \tag{24}
\end{aligned}$$

Plugging into Eqn.9 leads to the many body pairing length  $\xi_i$  along different directions versus the SOC strength shown in Fig.2. We also plot a reference line  $k_F \xi_0 = \hbar$  ( $k_F \xi_{0i} = \frac{\hbar}{\sqrt{3}}$  for each component) to qualitatively signal the BCS to BEC crossover. As shown in the Fig.2, the pairing length in both  $x$  (or  $y$ ) and  $z$  direction decrease monotonically and sharply as the SOC strength increases for a fixed interaction strength  $\frac{\hbar}{k_F a_s}$ , and finally drop below the reference line. This is the most direct evidence that the Rashba SOC drives a crossover from BCS to BEC. The monotonic decreasing shape of the pairing length in Fig.2 can be directly detected by radio-frequency dissociation spectra experiment<sup>38</sup>.

In the absence of the SOC when  $\lambda = 0$ , there is only a singlet pairing, one can get an analytical result:

$$\begin{aligned}
\xi_{x,y,z}^2(\lambda = 0) &= \frac{\hbar^2 \int dp p^{d+1} \frac{\xi_p^2}{E_p^6}}{d(2m)^2 \int dp \frac{p^{d-1}}{E_p^2}} \\
&= \frac{\hbar^2 \sqrt{\frac{\eta(16\eta^4 + 52\eta^2 + 45)}{\eta^2 + 1} + \frac{16\eta^4 + 44\eta^2 + 25}{\sqrt{\eta^2 + 1}}}}{(2m\Delta) 24\sqrt{\eta + \sqrt{\eta^2 + 1}}} \tag{25}
\end{aligned}$$

where  $\eta = \frac{\mu}{\Delta}$ . In the weak coupling (BCS) limit<sup>37</sup>  $\frac{\hbar}{k_F a_s} \rightarrow -\infty$ ,  $\mu = E_F$  and  $\Delta_0 = \frac{8E_F}{e^2} e^{\frac{\pi\hbar}{2k_F a_s}} \rightarrow 0$ ,  $\xi_{x,y,z} = \frac{1}{\sqrt{6}} \frac{\hbar k_F}{2m\Delta_0} = \frac{1}{\sqrt{6}} \xi_{0BCS}$  where  $\xi_{0BCS} = \frac{\hbar v_F}{2\Delta_0}$  is nothing but the coherence length<sup>28</sup> which goes to  $\infty$  as  $\frac{\hbar}{k_F a_s} \rightarrow -\infty$ . In the strong coupling (BEC) limit<sup>37</sup>  $\frac{\hbar}{k_F a_s} \rightarrow \infty$ ,  $\mu = -\frac{E_b}{2} + \frac{2k_F a_s}{3\pi\hbar} E_F$  where  $E_b = \frac{1}{ma_s^2}$  is the binding energy, the  $\Delta_0 = \sqrt{\frac{16\hbar}{\pi k_F a_s} E_F}$ , so  $\xi_{x,y,z} \rightarrow \frac{a_s}{\sqrt{6}}$  which recovers the two-body scattering length Eqn.32<sup>40</sup>.

The pairing lengths along different directions versus the scattering length is shown in Fig.3 which is complementary to Fig.2.

### C. Cooper pair size across BCS to BEC crossover

As shown in Sec.II, the Cooper pair size in Eqn.14 is another characteristic length in Fermi gas system. Formally, one can define the ‘‘Cooper pair wavefunction’’<sup>15</sup> in the second quantized form by removing the exponen-

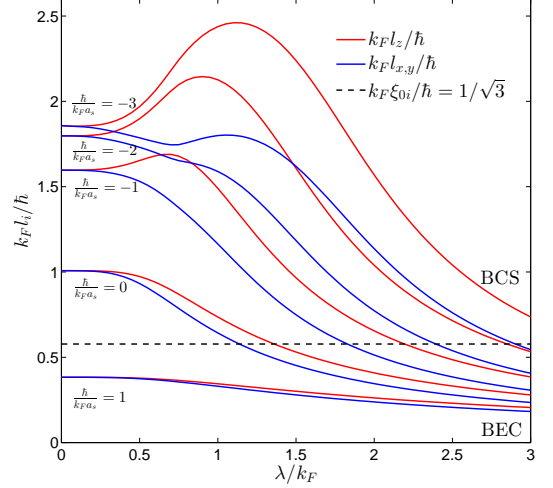


FIG. 4. The Cooper pair size defined in Eqn.14 29 along  $x$  direction (red lines) ( $l_x = l_y$ ) and  $z$  direction (blue lines) as a function of 3d Rashba SOC strength  $\lambda$ . Note its non-monotonic behaviors in the BCS side. The effects of SOC are small starting from the BEC side at  $\lambda = 0$ .

tial in Eqn.21:

$$\begin{aligned}
|g_{cp}\rangle &= \sum_{\mathbf{p}}' \left[ w_{\mathbf{p}+} e^{-i\varphi_{\mathbf{p}}} h_{\mathbf{p}+}^\dagger h_{-\mathbf{p}+}^\dagger + w_{\mathbf{p}-} e^{i\varphi_{\mathbf{p}}} h_{\mathbf{p}-}^\dagger h_{-\mathbf{p}-}^\dagger \right] |0\rangle \\
&= \sum_{\mathbf{p}}' [g_{\uparrow\downarrow}(\mathbf{p}) c_{\mathbf{p}\uparrow}^\dagger c_{-\mathbf{p}\downarrow}^\dagger + g_{\downarrow\uparrow}(\mathbf{p}) c_{\mathbf{p}\downarrow}^\dagger c_{-\mathbf{p}\uparrow}^\dagger \\
&\quad + g_{\uparrow\uparrow}(\mathbf{p}) c_{\mathbf{p}\uparrow}^\dagger c_{-\mathbf{p}\uparrow}^\dagger + g_{\downarrow\downarrow}(\mathbf{p}) c_{\mathbf{p}\downarrow}^\dagger c_{-\mathbf{p}\downarrow}^\dagger] |0\rangle, \tag{26}
\end{aligned}$$

which only has two paired electrons with both singlet and triplet pairing. In Eqn.26, we have used Eqn.17 and found:

$$\begin{aligned}
g_{\uparrow\downarrow}(\mathbf{p}) &= -\frac{1}{2} (w_{\mathbf{p}+} + w_{\mathbf{p}-}) = -g_{\downarrow\uparrow}(-\mathbf{p}) = -g_{\downarrow\uparrow}(\mathbf{p}), \\
g_{\uparrow\uparrow}(\mathbf{p}) &= \frac{1}{2} (w_{\mathbf{p}+} - w_{\mathbf{p}-}) e^{-i\varphi_{\mathbf{p}}} = -g_{\downarrow\downarrow}^*(\mathbf{p}). \tag{27}
\end{aligned}$$

The corresponding first quantized form of Eqn.26 in real space is:

$$\begin{aligned}
g_{cp}(\vec{r}) &= g_{\uparrow\downarrow}(\vec{r}) (|\uparrow\downarrow\rangle - |\downarrow\uparrow\rangle) \\
&\quad + g_{\uparrow\uparrow}(\vec{r}) |\uparrow\uparrow\rangle - g_{\downarrow\downarrow}^*(\vec{r}) |\downarrow\downarrow\rangle, \tag{28}
\end{aligned}$$

where  $g_{\alpha\beta}(\vec{r}) = \sum_{\vec{p}} e^{i\vec{p}\cdot\vec{r}} g_{\alpha\beta}(\vec{p})$ ,  $\alpha, \beta = \uparrow, \downarrow$ . Compared to Eqn.11, one can see that there are two extra equal-spin  $p_x \pm ip_y$  pairing components<sup>29</sup> similar to the  $A$ -phase of  $^3\text{He}$ .

It is easy to see that the Cooper pair size along the  $i$  direction in Eqn.14 can be expressed as:

$$l_i^2 = \frac{\langle g_{cp} | r_i^2 | g_{cp} \rangle}{\langle g_{cp} | g_{cp} \rangle}, \quad i = x, y, z, \tag{29}$$

which has a clear physical meaning: the Cooper pair size is the ‘‘average size’’ of the Cooper pair wavefunction

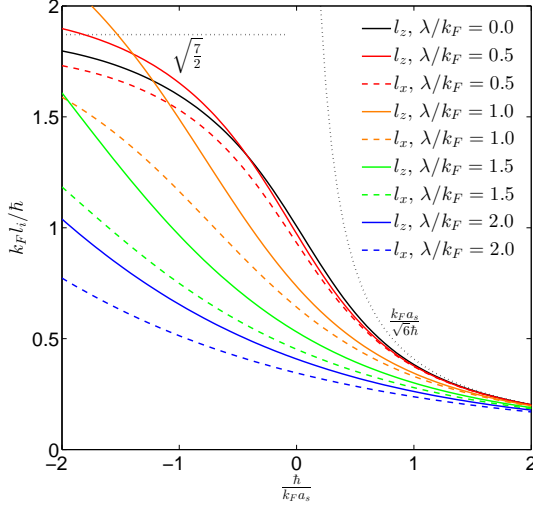


FIG. 5. The Cooper pair size  $l_z > l_x = l_y$  at a fixed 3d Rashba SOC versus the scattering length. Different colors stand for different SOC strengths. Solid (dashed) lines stand for  $l_z$  ( $l_x = l_y$ ). The dark dotted line on the left (right) is its BCS (BEC) limit  $\sqrt{7/2}$  ( $\frac{k_F a_s}{\sqrt{6\hbar}}$ ) at  $\lambda = 0$ . On the BCS side, the SOC effects are dramatic, but on the BEC side, the SOC effects are small, all curves converge to the right dotted line  $\frac{k_F a_s}{\sqrt{6\hbar}}$  from below.

Eqn.28. Shown in Fig.4 is the the Cooper pair size along different directions versus the SOC strength. In sharp contrast to the pairing length, it is non-monotonic<sup>41</sup> in the BCS side  $a_s < 0$ , so may not be a good quantity to characterize the BCS to BEC crossover. Furthermore, it may not be an experimentally detectable quantity anyway.

In the absence of the SOC when  $\lambda = 0$ , there is only a singlet pairing, Eqn.29 is simplified to:

$$l_i^2(\lambda = 0) = \frac{\hbar^2 \sum_{\mathbf{k}} \left(1 - \frac{\xi_{\mathbf{k}}}{E_{\mathbf{k}}}\right)^2 \frac{k^2}{m^2}}{3 \sum_{\mathbf{k}} (E_{\mathbf{k}} - \xi_{\mathbf{k}})^2}. \quad (30)$$

In the weak coupling (BCS) limit (i.e.  $\frac{\hbar}{k_F a_s} \rightarrow -\infty$ ),  $\mu = E_F$  and  $\Delta \rightarrow 0$ , one finds  $l_{x,y,z} \rightarrow \sqrt{\frac{7}{2}} \frac{\hbar}{k_F}$  which is nothing but the inter-particle distance, in sharp contrast to the pairing length which is nothing but the coherence length. Using  $l_{0BCS} \sim \frac{\hbar^2 k_F}{2m\epsilon_F}$ ,  $\xi_{0BCS} \sim \frac{\hbar^2 k_F}{2m\Delta_0}$ , one can see their ratio  $l_{0BCS}/\xi_{0BCS} \sim \Delta_0/\epsilon_F = \frac{8}{e^2} e^{\frac{\pi\hbar}{2k_F a_s}} \rightarrow 0$ . For conventional superconductors  $l_{0BCS}/\xi_{0BCS} \sim 10^{-4}$  which indicates that there are about  $10^4$  other Cooper pairs inside a given Cooper pair. However, for high  $T_c$  superconductors<sup>29,31</sup>,  $l_{0BCS}/\xi_{0BCS} \sim 10^{-1}$  which indicates that they are quite close to the BCS to BEC crossover, but still in the BCS side.

In the BEC limit, we find  $l_i \rightarrow \frac{a_s}{\sqrt{6}}$  which also recovers the two-body scattering length Eqn.32<sup>40</sup>. So

$l_{0BCS}/\xi_{0BCS} = 1$  in the strong BEC limit. This should be expected because the Cooper pair wavefunction is nothing but the two electrons component of the many-body wavefunction, so both lengths have to be the same in the strong BEC limit.

The Cooper pair sizes along different directions versus the scattering length is shown in Fig.5 which is complementary to Fig.4

#### D. Contrast with two-body wavefunctions

The 2-body wavefunction with a 3d Rashba SOC was worked out in<sup>14</sup> by solving a 2-body Schrodinger equation<sup>28</sup>. It is instructive to compare the many-body wave functions Eqn.21 and the Cooper pair wavefunction Eqn.27 with the corresponding two-body wave functions (see the extreme oblate case in<sup>14</sup>). They all have the same symmetries, namely:

$$\begin{aligned} \psi_{\uparrow\downarrow}(\mathbf{p}) &= -\psi_{\downarrow\uparrow}(\mathbf{p}), & g_{\uparrow\downarrow}(\mathbf{p}) &= -g_{\downarrow\uparrow}(\mathbf{p}), \\ \psi_{\uparrow\uparrow}(\mathbf{p}) &= -\psi_{\downarrow\downarrow}^*(\mathbf{p}), & g_{\uparrow\uparrow}(\mathbf{p}) &= -g_{\downarrow\downarrow}^*(\mathbf{p}). \end{aligned} \quad (31)$$

However, they have quite different behaviors. It was shown that in the absence of the SOC when  $\lambda = 0$ , there exist a bound state in the BEC side only with  $a_s > 0$ , the bound state has only a singlet component  $\psi_0(\vec{r}) = \frac{1}{r} e^{-r/a_s}$  with a binding energy  $E_b = \frac{\hbar^2}{ma_s}$ . It is easy to see the size of the bound state:

$$b(\lambda = 0) = \frac{\langle \psi_0 | r^2 | \psi_0 \rangle}{\langle \psi_0 | \psi_0 \rangle} = \frac{a_s}{\sqrt{2}}, \quad (32)$$

which is identical to both the pairing size Eqn.9 and the Cooper-pair size Eqn.14 in the BEC limit<sup>40</sup>. As shown in Fig.1, in the absence of the SOC when  $\lambda = 0$ , the pairing length  $\xi_i$  and Cooper pair size  $l_i$  are well defined in both the BCS and BEC limit.

However, as shown in<sup>14</sup>, a non-zero SOC strength  $\lambda \neq 0$  will always lead to a two-body bound state at any  $a_s$ , extending the  $b(\lambda = 0)$  in Eqn.32 to a non-zero  $\lambda$  can be easily calculated using the two body wavefunctions in<sup>14,20</sup>. Any non-zero SOC strength, as shown in Fig.1, leads to  $\xi_z > \xi_x = \xi_y$  and  $l_z > l_x = l_y$ . In the BCS side,  $\xi_i$  and  $l_i$  display dramatically different behaviors. While in the BEC limit both  $\xi_i$  and  $l_i$  converge to the size of the two-body bound state. This is expected, in the strong BEC limit, the overlap between the two-body wavefunction and the many-body wavefunction must be the same as that between the two-body wavefunction and the Cooper-pair wavefunction.



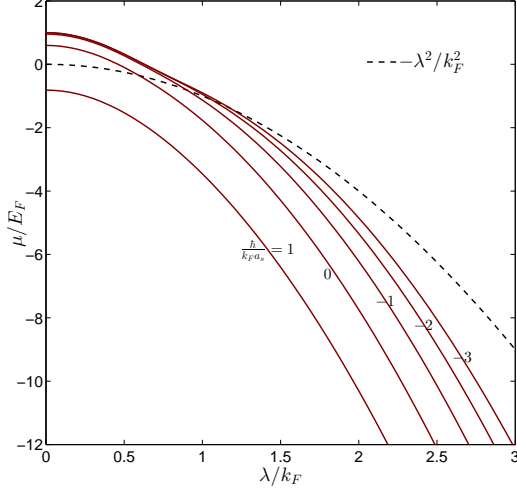


FIG. 6. The chemical potential  $\mu$  versus the 3D isotropic Weyl SOC strength  $\lambda$  for different scattering lengths. The black dashed line  $\mu_0 = -\frac{\lambda^2}{2m}$  is the chemical potential at the bottom of single particle spectrum. Starting from the BCS side at  $\lambda = 0$ , as  $\lambda$  increases, the  $\mu$  drops below  $\mu_0$  indicating a crossover from BCS to BEC.

#### IV. 3D FERMION GAS WITH AN ISOTROPIC WEYL SOC

The 3d Weyl SOC term can be written as

$$V_{Weyl} = \frac{\lambda}{m} \sum_{\mathbf{p}} [p_{\perp} (e^{-i\varphi_{\mathbf{p}}} c_{\mathbf{p}\uparrow}^{\dagger} c_{\mathbf{p}\downarrow} + e^{i\varphi_{\mathbf{p}}} c_{\mathbf{p}\downarrow}^{\dagger} c_{\mathbf{p}\uparrow}) + p_z (c_{\mathbf{p}\uparrow}^{\dagger} c_{\mathbf{p}\uparrow} - c_{\mathbf{p}\downarrow}^{\dagger} c_{\mathbf{p}\downarrow})]. \quad (33)$$

The single particle part in Hamiltonian Eqn.1 can be diagonalized in the helicity bases as  $H_0 = \sum_{\mathbf{p}} (\xi_{\mathbf{p}+} h_{\mathbf{p}+}^{\dagger} h_{\mathbf{p}+} + \xi_{\mathbf{p}-} h_{\mathbf{p}-}^{\dagger} h_{\mathbf{p}-})$  where  $\xi_{\mathbf{p}\pm} = \frac{p^2}{2m} \pm \frac{\lambda p}{m} - \mu$  and the helicity operators:

$$h_{\mathbf{p}+} = \sqrt{\frac{1}{2}} \left[ \sqrt{\frac{p+p_z}{p}} c_{\mathbf{p}\uparrow} + \sqrt{\frac{p-p_z}{p}} e^{-i\varphi_{\mathbf{p}}} c_{\mathbf{p}\downarrow} \right], \\ h_{\mathbf{p}-} = \sqrt{\frac{1}{2}} \left[ \sqrt{\frac{p-p_z}{p}} e^{i\varphi_{\mathbf{p}}} c_{\mathbf{p}\uparrow} - \sqrt{\frac{p+p_z}{p}} c_{\mathbf{p}\downarrow} \right]. \quad (34)$$

In the mean-field theory, the total Hamiltonian can also be diagonalized as Eqn.18, and the quasiparticle excitation energy  $E_{\mathbf{p}\pm} = \sqrt{\xi_{\mathbf{p}\pm}^2 + |\Delta_0|^2}$ , and the Bogoliubov quasi-particle operators take the same form as Eqn.19. At zero temperature, the two self-consistent equations also take the same form as Eqn.20 with the corresponding  $\xi_{\mathbf{p}\pm}$  and  $E_{\mathbf{p}\pm}$  defined above. Solving them leads to the chemical potential shown in Fig.6. Similar to Fig.1, the Weyl SOC also drives a new crossover from BCS to BEC.

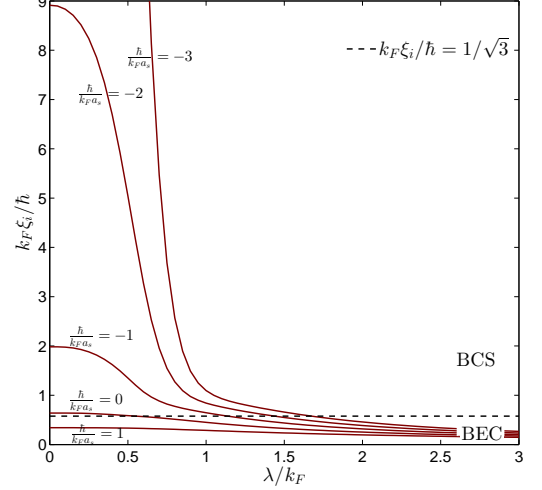


FIG. 7. From the BCS side at  $\lambda = 0$ , the pairing length  $\xi_x = \xi_y = \xi_z$  of 3d Weyl SOC decreases quickly and monotonically as the  $\lambda$  increases and drop below the dashed line. It describes precisely the new BCS to BEC crossover driven by the SOC strength. The dashed line is a contrasting line where  $k_F \xi_0 = \hbar$  (for each component,  $k_F \xi_{0i} = \hbar/\sqrt{3}$ ). From the BEC side at  $\lambda = 0$ , the effects of SOC are small.

##### A. Pairing length

The wavefunction stays the same as Eqn.21 with the corresponding  $\xi_{\mathbf{p}\pm}$  and  $E_{\mathbf{p}\pm}$  defined above. Similar to Sec.III-B, we can determine the singlet pairing amplitude:

$$\psi_{\uparrow\downarrow}(\mathbf{p}) = \frac{\langle BCS | c_{\mathbf{p}\uparrow}^{\dagger} c_{-\mathbf{p}\downarrow}^{\dagger} | BCS \rangle}{\langle BCS | BCS \rangle} \\ = \mp \frac{1}{2} \left( \frac{w_{\mathbf{p}+}}{1 + w_{\mathbf{p}+}^2} + \frac{w_{\mathbf{p}-}}{1 + w_{\mathbf{p}-}^2} \right) \\ - \frac{1}{2} \left( \frac{w_{\mathbf{p}+}}{1 + w_{\mathbf{p}+}^2} - \frac{w_{\mathbf{p}-}}{1 + w_{\mathbf{p}-}^2} \right) \frac{p_z}{p},$$

and triplet pairing amplitude:

$$\psi_{\uparrow\uparrow}(\mathbf{p}) = \frac{\langle BCS | c_{\mathbf{p}\uparrow}^{\dagger} c_{-\mathbf{p}\uparrow}^{\dagger} | BCS \rangle}{\langle BCS | BCS \rangle} \\ = \frac{1}{2} \left( \frac{w_{\mathbf{p}+}}{1 + w_{\mathbf{p}+}^2} - \frac{w_{\mathbf{p}-}}{1 + w_{\mathbf{p}-}^2} \right) \frac{p_{\perp}}{p} e^{i\varphi_{\mathbf{p}}} = -\psi_{\downarrow\downarrow}^*(\mathbf{p}),$$

where  $w_{\mathbf{p}\pm} = \sqrt{\frac{E_{\mathbf{p}\pm} - \xi_{\mathbf{p}\pm}}{E_{\mathbf{p}\pm} + \xi_{\mathbf{p}\pm}}}$ .

The pairing length  $\xi_i$  can be calculated using Eqn.9 and is shown in Fig.7. As the Weyl SOC strength increases, in the BCS side, the pairing length along any direction decreases monotonically and quickly, then drops below the dashed line. In the BEC side, the effects of the SOC strength are quite small. This is the most direct evidence that the Weyl SOC can also drive a crossover



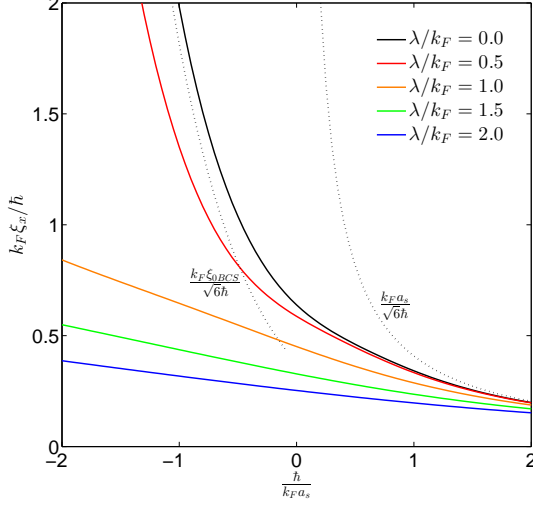


FIG. 8. The pairing lengths  $\xi_i$  of 3d Weyl SOC at a fixed SOC versus the scattering length. Different colors stand for different SOC strengths. The dark dotted line on the left (right) is its BCS (BEC) limit  $\frac{1}{\sqrt{6}} k_F \xi_{0BCS} = \frac{1}{8\sqrt{6}e^2} e^{-\frac{\pi\hbar}{2k_F a_s}} (\frac{k_F a_s}{\sqrt{6}})$  at  $\lambda = 0$ . On the BCS side, the SOC effects are dramatic, but on the BEC side, the SOC effects are small, all curves converge to the right dotted line  $\frac{k_F a_s}{\sqrt{6}}$  from below. Compare with Fig.3.

from BCS to BEC and can be directly detected by the MIT type of experiment<sup>38</sup>.

The pairing lengths versus the scattering length is shown in Fig.8 which is complementary to Fig.7

### B. Cooper pair size

The Cooper pair wave function takes the same form as Eqn.26 in the second quantized form and Eqn.28 in the first quantized form with the corresponding  $\xi_{p\pm}$  and  $E_{p\pm}$  defined above. All the components can be written as:

$$\begin{aligned} g_{\uparrow\downarrow}(\mathbf{p}) &= -\frac{1}{2}(w_{\mathbf{p}+} + w_{\mathbf{p}-}) - \frac{1}{2}(w_{\mathbf{p}+} - w_{\mathbf{p}-}) \frac{p_z}{p} = -g_{\uparrow\downarrow}(-\mathbf{p}) \\ g_{\downarrow\uparrow}(\mathbf{p}) &= \frac{1}{2}(w_{\mathbf{p}+} + w_{\mathbf{p}-}) - \frac{1}{2}(w_{\mathbf{p}+} - w_{\mathbf{p}-}) \frac{p_z}{p}, \\ g_{\uparrow\uparrow}(\mathbf{p}) &= \frac{1}{2}(w_{\mathbf{p}+} - w_{\mathbf{p}-}) \frac{p_{\perp}}{p} e^{-i\varphi_{\mathbf{p}}} = -g_{\downarrow\downarrow}^*(\mathbf{p}). \end{aligned} \quad (35)$$

The Cooper-pair size can be evaluated using Eqn.29 and plotted in Fig.9. Its non-monotonic behaviors at the BCS side indicate it may not be a good quantity to characterize the crossover.

The Cooper pair sizes versus the scattering length is shown in Fig.10 which is complementary to Fig.9.

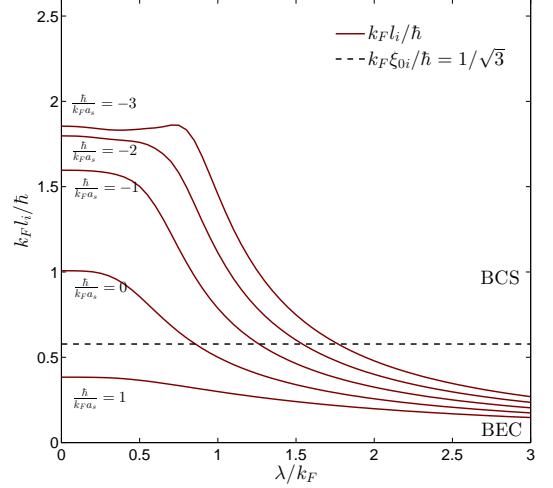


FIG. 9. The Cooper pair size  $l_x = l_y = l_z$  of 3d Weyl SOC as a function of  $\lambda$ . Note its non-monotonic behavior at the BCS side. The SOC effects on the BEC side are small.

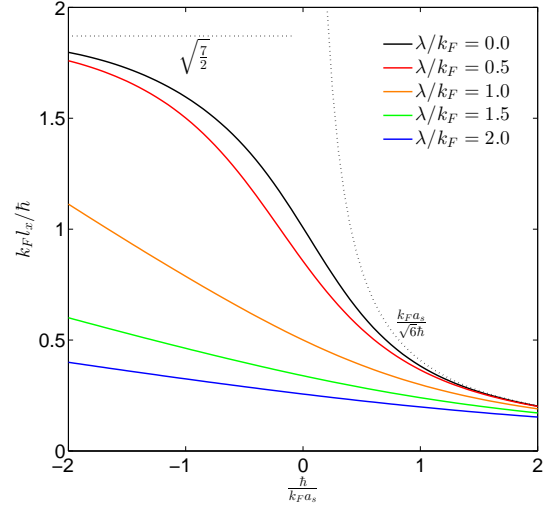


FIG. 10. The Cooper pair size  $l_i$  of 3d Weyl SOC at a fixed SOC versus the scattering length. Different colors stand for different SOC strengths. The dark dotted line on the left (right) is its BCS (BEC) limit  $\sqrt{7/2} (\frac{k_F a_s}{\sqrt{6}})$  at  $\lambda = 0$ . On the BCS side, the SOC effects are dramatic, but on the BEC side, the SOC effects are small, all curves converge to the right dotted line  $\frac{k_F a_s}{\sqrt{6}}$  from below. Compare with Fig.5.

### C. Contrast with the two-body wavefunctions

To explore the relations between the many-body wavefunctions or the “Cooper-pair” wavefunction studied in this section and the two body wavefunctions in<sup>14</sup>, it is convenient to introduce the spin eigenstate along the mo-

mentum  $\frac{\mathbf{p}}{p} = (\sin \theta \cos \varphi, \sin \theta \sin \varphi, \cos \theta)$ :

$$\begin{aligned} |\uparrow\rangle_{\mathbf{p}} &= e^{-i\frac{\varphi}{2}} \cos \frac{\theta}{2} |\uparrow\rangle + e^{i\frac{\varphi}{2}} \sin \frac{\theta}{2} |\downarrow\rangle, \\ |\downarrow\rangle_{\mathbf{p}} &= e^{-i\frac{\varphi}{2}} \sin \frac{\theta}{2} |\uparrow\rangle - e^{i\frac{\varphi}{2}} \cos \frac{\theta}{2} |\downarrow\rangle, \end{aligned}$$

then to express the many-body wavefunctions in terms of the spin eigenstates along the momentum  $\vec{p}$ :

$$\begin{aligned} & g_{\uparrow\downarrow}(\mathbf{p}) |\uparrow\downarrow\rangle + g_{\downarrow\uparrow}(\mathbf{p}) |\downarrow\uparrow\rangle + g_{\uparrow\uparrow}(\mathbf{p}) |\uparrow\uparrow\rangle + g_{\downarrow\downarrow}(\mathbf{p}) |\downarrow\downarrow\rangle \\ &= -\frac{1}{2} (w_{p+} + w_{p-}) (|\uparrow\downarrow\rangle - |\downarrow\uparrow\rangle) + \frac{1}{2} (w_{p+} - w_{p-}) \times \\ & \quad \left[ \frac{p_x - ip_y}{p} |\uparrow\uparrow\rangle - \frac{p_z}{p} (|\uparrow\downarrow\rangle + |\downarrow\uparrow\rangle) - \frac{p_x + ip_y}{p} |\downarrow\downarrow\rangle \right] \\ &= -\frac{1}{2} (w_{p+} + w_{p-}) (|\uparrow\downarrow\rangle - |\downarrow\uparrow\rangle) \\ & \quad + \frac{1}{2} (w_{p+} - w_{p-}) (|\uparrow\downarrow\rangle_{\mathbf{p}} + |\downarrow\uparrow\rangle_{\mathbf{p}}) \\ &\equiv g_a(p) (|\uparrow\downarrow\rangle - |\downarrow\uparrow\rangle) + g_s(p) (|\uparrow\downarrow\rangle_{\mathbf{p}} + |\downarrow\uparrow\rangle_{\mathbf{p}}), \quad (36) \end{aligned}$$

where the components  $g_a(p)$  and  $g_s(p)$  are independent on direction of  $\mathbf{p}$  (i.e.  $\theta$  and  $\varphi$ ). Compared to Eqn.11, one can see that there are three extra  $p_x \pm ip_y$  and  $p_z$  pairing components<sup>29</sup> similar to the *B*-phase of superfluid  $^3\text{He}$ . This fact should be contrasted to Eqn.28 where there are only two extra equal-spin  $p_x \pm ip_y$  pairing components<sup>29</sup> similar to the *A*-phase of superfluid  $^3\text{He}$ .

Fourier transforming the ‘‘Cooper-pair’’ wavefunction Eqn.36 to real space and comparing with the two body wavefunction in the spherical case in<sup>14</sup>, we find that they have the same symmetry. In fact, a similar relation between the wavefunctions (or order parameters) in real space and those in the helicity momentum basis were derived for magnetic transitions in repulsively interacting Fermi gas<sup>23</sup>.

## V. 2D FERMI GAS WITH A RASHBA SOC

A 2D Rashba SOC term can be written as

$$V_{2d-ra} = \frac{\lambda}{m} \sum_{\mathbf{p}} p \left[ e^{-i\varphi_{\mathbf{p}}} c_{\mathbf{p}\uparrow}^\dagger c_{\mathbf{p}\downarrow} + e^{i\varphi_{\mathbf{p}}} c_{\mathbf{p}\downarrow}^\dagger c_{\mathbf{p}\uparrow} \right], \quad (37)$$

where  $\lambda$  is the strength of SOC,  $p = \sqrt{p_x^2 + p_y^2}$  and  $\varphi_{\mathbf{p}} = \text{Arg}(p_x + ip_y)$ . Note that the space is 2d, but the spin is still  $SU(2)$  with the 3 generators.

The BCS theory in two dimension has been studied by several works<sup>42,43</sup> with different focus. The calculations are similar to the 3d Rashba case in Sec.III with the momentum  $\vec{p}$  confined to be the 2d momentum  $\vec{p}_\perp$ , or similar to the 3d Weyl case in Sec.IV by setting  $p_z = 0$ . Eqn.16,17, 18, 19 follow. The two self-consistent equations Eqn.20 also hold with the crucial difference that the interaction need to be regularized by a bound state energy  $\epsilon_B$  at 2d, instead of a scattering length  $a_s$  in 3d:

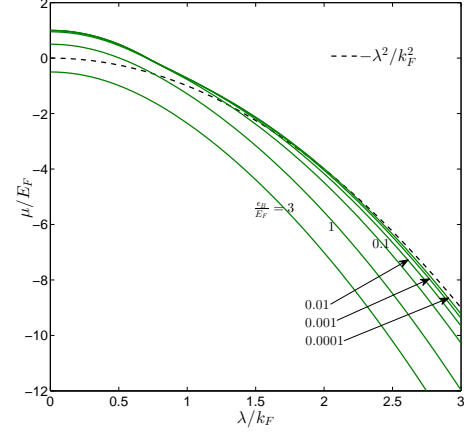


FIG. 11. The chemical potential  $\mu$  versus  $\lambda$  in 2D isotropic SOC system for different scattering lengths. The dashed line is the minimum energy of the single particle  $\mu_0 = -\frac{\lambda^2}{2m}$ . On the BCS side, as  $\lambda$  increases, the  $\mu$  drops below  $\mu_0$  indicating a crossover from a BCS to BEC crossover.

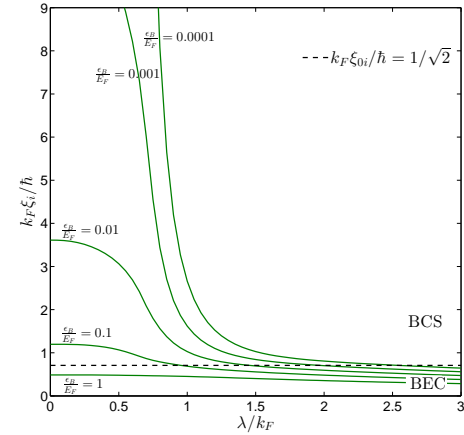


FIG. 12. The 2d pairing length defined in Eqn.9 ( $\xi_x = \xi_y$ ) as a function of  $\lambda$ . At the BCS side, it decreases quickly and monotonically as the  $\lambda$  increases and drop below the dashed line. It describe precisely the new BCS to BEC crossover driven by the SOC strength. The dashed line is a guidance line where  $k_F \xi_0 = \hbar$  (averagely,  $k_F \xi_{0i} = \hbar/\sqrt{2}$ ). At the BEC side, the effects of SOC are small.

$\frac{1}{g} = -\frac{1}{V} \sum_{\mathbf{p}} \frac{1}{2\epsilon_{\mathbf{p}} + \epsilon_B}$ . Solving them leads to the chemical potential  $\mu$  shown in Fig.11.

### A. Pairing length

When calculating the pairing length, Eqns.21, 23, 24 still hold. For  $\lambda \neq 0$ , only numerical results are available and are shown in Fig.12. We can see that in the BCS limit at  $\lambda = 0$ , as the strength of SOC increases for a fixed

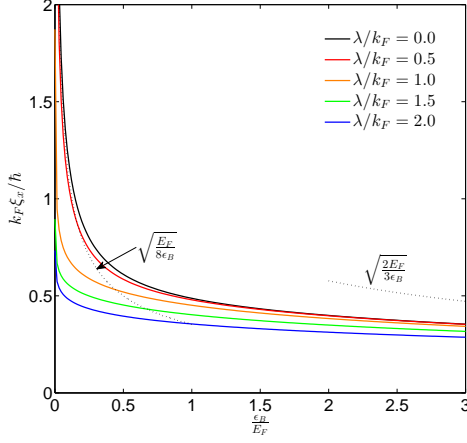


FIG. 13. The 2d pairing lengths  $\xi_x = \xi_y$  at a fixed SOC versus the scattering length. Different colors stand for different SOC strengths. The black dotted line on the left (right) is its BCS (BEC) limit  $\sqrt{\frac{E_F}{8\epsilon_B}}$  ( $\sqrt{\frac{2E_F}{3\epsilon_B}}$ ) at  $\lambda = 0$ . On the BCS side, the SOC effects are dramatic, but on the BEC side, the SOC effects are small, all curves converge to the right dotted line  $\sqrt{\frac{2E_F}{3\epsilon_B}}$  from below.

interaction strength  $\frac{\epsilon_B}{E_F}$ , the pair size decreases monotonically and sharply, then below the reference line. Here, we also plot a reference line by taking  $k_F \xi_0 = \hbar$  (for each component,  $k_F \xi_{0i} = \frac{\hbar}{\sqrt{2}}$ ) to qualitatively observe the BCS to BEC crossover behavior. In the BEC limit, the effects of SOC are small.

Setting  $\lambda = 0$ , one can easily solve the self-consistent equations and find  $\mu = E_F - \frac{|\epsilon_B|}{2}$  and  $\Delta = \sqrt{2|\epsilon_B|E_F}$ . When  $\lambda = 0$ , Eqn.25 at  $d = 3$  should be replaced by<sup>42,43</sup>:

$$\begin{aligned} \xi_{x,y}^2(\lambda = 0) &= \frac{\hbar^2 4 \int dp p^{d+1} \frac{\xi_p^2}{E_p^6}}{(2m)^2 d \int dp \frac{p^{d-1}}{E_p^2}} \\ &= \frac{\hbar^2}{4(2m\Delta)} \left( \eta + \frac{\eta^2 + 2}{\eta^2 + 1} \frac{1}{\frac{\pi}{2} + \arctan \eta} \right) \end{aligned} \quad (38)$$

where  $\eta = \frac{\mu}{\Delta}$ . Because of different dimensions, this analytical expression is very different from Eqn.25 in 3d. In the BCS limit (i.e.  $\frac{\epsilon_B}{E_F} \rightarrow 0$ ),  $\eta = \frac{1}{\sqrt{2}} \sqrt{\frac{E_F}{|\epsilon_B|}} \rightarrow \infty$ ,  $k_F \xi_{x,y} \rightarrow \sqrt{\frac{E_F}{8|\epsilon_B|}}$  which diverges. In the BEC limit (i.e.  $\frac{|\epsilon_B|}{E_F} \rightarrow \infty$ ),  $\mu = -\frac{|\epsilon_B|}{2}$  and  $\eta = -\frac{1}{2\sqrt{2}} \sqrt{\frac{|\epsilon_B|}{E_F}} \rightarrow -\infty$ ,  $k_F \xi_{x,y} \rightarrow \sqrt{\frac{3}{2} \frac{E_F}{|\epsilon_B|}}$ .

Shown in Fig.13 is the pairing length versus the scattering length which is complementary to Fig.12.

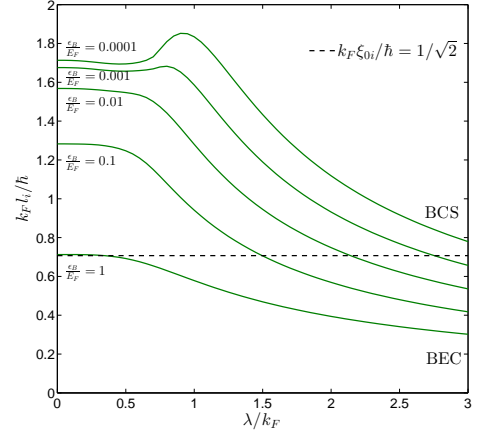


FIG. 14. The 2d Cooper pair size  $l_x = l_y$  as a function of  $\lambda$ . Note its non-monotonic behavior at the BCS side.

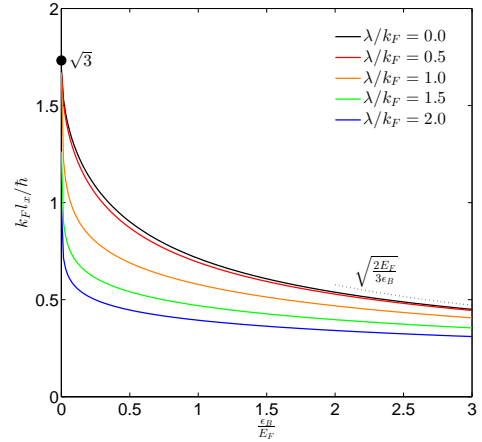


FIG. 15. The 2d Cooper pair size  $l_x = l_y$  at a fixed SOC versus the scattering length. Different colors stand for different SOC strengths. The black dotted line on the left (right) is its BCS (BEC) limit  $\sqrt{3}$  ( $\sqrt{\frac{2E_F}{3\epsilon_B}}$ ) at  $\lambda = 0$ . On the BCS side, the SOC effects are dramatic, but on the BEC side, the SOC effects are small, all curves converge to the right dotted line  $\sqrt{\frac{2E_F}{3\epsilon_B}}$  from below.

## B. Cooper pair size

When calculating the Cooper-pair size, Eqns. 26, 27, 28, 29 still hold. Shown in Fig.14 is how the Cooper-pair size changes with  $\lambda$ . Once more, its non-monotonic behaviors at the BCS side indicate it may not be a good quantity to characterize the BCS to BEC crossover.

When  $\lambda = 0$ , Eqn.30 at  $d = 3$  should be replaced by:

$$l_i^2(\lambda = 0) = \frac{3\hbar^2 \left[ \ln 2 - \frac{1}{2} - \eta \left( \frac{\pi}{2} + \arctan \eta \right) - \ln \left( 1 - \frac{\eta}{\sqrt{\eta^2 + 1}} \right) + \eta \left( \eta + \sqrt{\eta^2 + 1} \right) \right]}{2m\Delta \left[ \eta^3 + (\eta^2 + 1)^{\frac{3}{2}} + \frac{3}{2}\eta \right]}, \quad (39)$$

where  $\eta = \frac{\mu}{\Delta}$ . In the BCS limit (i.e.  $\frac{\epsilon_B}{E_F} \rightarrow 0$ ), one get  $l_{x,y} \rightarrow \sqrt{3} \frac{\hbar}{k_F}$  which is nothing but the inter-particle distance, so it goes to a finite value, in sharp contrast to the pairing length which diverges. In fact,  $l/\xi \sim \Delta_0/\epsilon_F \rightarrow 0$  in the BCS limit. In the BEC limit (i.e.  $\frac{\epsilon_B}{E_F} \rightarrow \infty$ ), one find  $k_F l_{x,y} = \sqrt{\frac{2E_F}{3|\epsilon_B|}}$  which is identical to  $k_F \xi_{x,y}$  in the BEC limit as it should be.

Shown in Fig.15 is the Cooper pair size at various fixed SOC strengths versus the bound state energies  $\epsilon_B/E_F$  which is complementary to Fig.14.

## VI. APPLICATIONS TO 2D SUPERCONDUCTOR AND SEMI-CONDUCTOR SYSTEMS

In various 3d condensed matter systems<sup>1,7</sup>, the 3d SOC usually take  $\lambda(\vec{k} \times \vec{\sigma}) \cdot \nabla V$  which is quite different form than Weyl or Rashba form studied in Sec.III and IV by keeping the inversion symmetry. It may be interesting to see if such a 3d inversion symmetric SOC can also drive a BCS to BEC crossover.

Eqn.1 with the 2D Rashba SOC term Eqn.37 may also describe 2d bright exciton with total angular momentum  $J = \pm 1$  in electron-hole semiconductor bilayer systems and electron pairings in 2d non-centrosymmetric superconductors<sup>2-4</sup>. It was known that in a 2d semiconductor electron gas, the 2d Rashba SOC strength depends on the electric field, presence of adatoms at the boundary, atomic weight and atomic shells involved<sup>2,5,6</sup>. In the surface of non-centrosymmetric superconductors, the strong near surface electric fields lead to a 2d Rashba SOC quite similar to the 2d superconducting fullerene and polyacene crystals in the field-effect-transistor geometry<sup>2</sup>. So the 2d Rashba SOC strength in the two condensed matter systems can also be tuned by adjusting various surface geometries. So the results achieved on the BCS to BEC crossover tuned by the 2d Rashba strength in the section V should also apply to these condensed matter systems. In Ref.<sup>32-35</sup>, the authors ignored the spins of the electrons and holes, therefore also the possible Rashba SOC. As shown at the end of<sup>34</sup>, the bright excitons couple to the one photon process with the polarization  $\sigma = \pm$ . By incorporating the coupling between the 2d bright excitons subject to the 2d Rashba SOC studied in Sec.V and the 3d emitted photons with the two polarizations, it is interesting study how the emitted photon characteristics change across the new BCS to BEC crossover driven by the 2d Rashba SOC.

## VII. DISCUSSIONS AND CONCLUSIONS

The new BCS to BEC crossover driven by the SOC strength has been studied by previous authors from the overlap between “Cooper-pair wavefunction” and two body wavefunction<sup>15</sup>, also from the “Cooper-pair size” right at the Feshbach resonance<sup>16</sup>. In this paper, we investigate the new BCS to BEC crossover from fundamental and physical points of view. At the mean field level, we studied the dependence of chemical potential, pairing length, Cooper-pair size on the SOC strength for three kinds of Fermi gases with 3d Rashba, 3d Weyl and 2d Rashba SOC respectively. We explicitly demonstrated the new BCS to BEC crossover driven by the SOC strength in all the three cases by monitoring the monotonic decreasing of chemical potential and the pairing length. We show that the most relevant wavefunction is the many body wave function instead of the “Cooper-pair wavefunction” or two body wavefunction, the most relevant length is the pairing length instead of the “Cooper-pair size” or the two-body bound state size. Among the three lengths, only the pairing length is the experimentally detectable length.

We can summarize the main differences among the pairing length, the Cooper-pair size and the two-body size in the following: In the absence of SOC, in the BCS limit, the pairing length goes to the coherence length  $\xi(\lambda = 0) = \hbar v_F/\Delta_0$ , while the Cooper-pair size goes to the inter-particle distance  $l(\lambda = 0) \sim 1/k_F$ . Their ratio  $l(\lambda = 0)/\xi(\lambda = 0) \sim \Delta_0/\epsilon_F$ . For conventional superconductors<sup>28</sup>,  $l(\lambda = 0)/\xi(\lambda = 0) \sim 10^{-4}$ , so they are well inside the BCS limit. The BCS mean field theory work well, quantum and classical fluctuation effects can be neglected except very close to the critical transitions at finite temperatures. For high temperature superconductors<sup>29,31</sup>,  $l(\lambda = 0)/\xi(\lambda = 0) \sim 10^{-1}$ , so they are quite close to BCS to BEC crossover, but still in the BCS limit with well defined Fermi surface. So quantum and classical fluctuation effects can not be ignored<sup>29</sup>. In the BEC limit, they both get to the two-body bound state size, therefore  $l(\lambda = 0)/\xi(\lambda = 0) \sim 1$ . The results on  $\xi$  in Eqn.25 at 3d<sup>37</sup> and Eqn.38 at 2d<sup>42,43</sup> are not new, but the results on  $l$  in Eqn.30 at 3d and Eqn.39 are new and show completely different behaviors than  $\xi$ . It is very instructive to compare the two different length scales. In the presence of SOC, on the BCS side, the pairing length  $\xi_i(\lambda)$ ,  $i = x, y, z$  decrease monotonically and quickly move into the BEC regime, so can be used to characterize the BCS to BEC crossover quantitatively. Furthermore it can be detected by RF dissociation spectra experiment. While  $l_i(\lambda)$  shows non-monotonic behaviors, so can not

be used to characterize the BCS to BEC crossover even qualitatively. Furthermore it is not an experimentally measurable quantity.

In a future publication, we will compute the fluctuation corrections to the mean field theory results on the pairing length achieved in this paper. One can achieve the goal by calculating the fermion pairing correlation function Eqn.8 using  $1/N$  expansion<sup>44,45</sup>. It was known the quantum fluctuation effects are important near the BCS to BEC regime. It may also be interesting to extend the zero temperature results on the pairing length to finite temperatures whose effects are especially important to 2d Rashba systems studied in Sec.V and VI. However, it is not known how to extend the concepts of Cooper-pair size defined in Eqn.14 beyond mean field results and to finite temperatures. Above all, its definition is based on the explicit form of the mean field state. Therefore, the pairing length is a much more robust concept than

the Cooper-pair size. It is also a experimentally measurable quantity through radio-frequency dissociation spectra. Of course, the two-body wavefunction is defined only for two fermions, can not be used to study a many body system anyway. The Cooper-pair size has been evaluated at the mean field through the topological transition in<sup>39</sup>. As demonstrated in this paper, the pairing length show quite different behaviors than the Cooper-pair size, it maybe useful to study the pairing length through various topological transitions driven by the Zeeman field<sup>46–48</sup>.

#### Acknowledgements

We thank Fadi Sun for helpful discussions. YY and JY are supported by NSF-DMR-1161497, NSFC-11174210, Beijing Municipal Commission of Education under Grant No. PHR201107121. WL was supported by the NKBRSCF under grants Nos. 2011CB921502, 2012CB821305, NSFC under grants Nos. 61227902, 61378017, 11311120053.

- 
- <sup>1</sup> Jinwu Ye, Y. B. Kim, A. J. Millis, B. I. Shraiman, P. Majumdar, and Z. Tešanović, *Phys. Rev. Lett.* **83**, 3737 (1999).
  - <sup>2</sup> Lev P. Gor'kov and Emmanuel I. Rashba, *Phys. Rev. Lett.* **87**, 037004 (2001).
  - <sup>3</sup> Wang Yao and Qian Niu, *Phys. Rev. Lett.* **101**, 106401 (2008).
  - <sup>4</sup> Wu Cong-Jun, Ian Mondragon-Shem, Zhou Xiang-Fa, *Chin. Phys. Lett.*, Vol. 28, 097102 (2011).
  - <sup>5</sup> M. Z. Hasan and C. L. Kane, *Rev. Mod. Phys.* **82**, 3045 (2010).
  - <sup>6</sup> X. L. Qi and S. C. Zhang, *Rev. Mod. Phys.* **83**, 1057 (2011).
  - <sup>7</sup> For example, see “Exotic Phases of Frustrated Magnets” conference held at KITP October 8-12, 2012. <http://online.kitp.ucsb.edu/online/fragnets-c12/>
  - <sup>8</sup> Y. J. Lin, K. Jiménez-García, and I. B. Spielman, *Nature (London)* **471**, 83 (2011).
  - <sup>9</sup> P. Wang, Z. Q. Yu, Z. Fu, J. Miao, L. Huang, S. Chai, H. Zhai, and J. Zhang, *Phys. Rev. Lett.* **109**, 095301 (2012).
  - <sup>10</sup> L. W. Cheuk, A. T. Sommer, Z. Hadzibabic, T. Yefsah, W. S. Bakr, and M. W. Zwierlein, *Phys. Rev. Lett.* **109**, 095302 (2012).
  - <sup>11</sup> For a review, see J. Dalibard, F. Gerbier, G. Juzeliūnas, and P. Öhberg, *Rev. Mod. Phys.* **83**, 1523 (2011).
  - <sup>12</sup> B. M. Anderson, I. B. Spielman, and G. Juzeliūnas, *Phys. Rev. Lett.* **111**, 125301 (2013).
  - <sup>13</sup> Z.-F. Xu, L. You, and M. Ueda, *Phys. Rev. A* **87**, 063634 (2013); Z. -F. Xu and L. You, *Phys. Rev. A* **85**, 043605 (2012).
  - <sup>14</sup> J. P. Vyasankere and V. B. Shenoy, *Phys. Rev. B* **83**, 094515 (2011).
  - <sup>15</sup> J. P. Vyasankere, S. Zhang and V. B. Shenoy, *Phys. Rev. B* **84**, 014512 (2011).
  - <sup>16</sup> Z. -Q. Yu and H. Zhai, *Phys. Rev. Lett.* **107**, 195305 (2011).
  - <sup>17</sup> H. Hu, L. Jiang, X. J. Liu and H. Pu, *Phys. Rev. Lett.* **107**, 195304 (2011).
  - <sup>18</sup> Lianyi He and Xu-Guang Huang, *Phys. Rev. Lett.* **108**, 145302 (2012).
  - <sup>19</sup> Kezhao Zhou and Zhidong Zhang, *Phys. Rev. Lett.* **108**, 025301 (2012) [5 pages]
  - <sup>20</sup> Lianyi He and Xu-Guang Huang, *Phys. Rev. B* **86**, 014511 (2012).
  - <sup>21</sup> Jayantha P. Vyasankere and Vijay B. Shenoy, *Phys. Rev. A* **86**, 053617 (2012).
  - <sup>22</sup> Shang-Shun Zhang, Xiao-Lu Yu, Jinwu Ye, Wu-Ming Liu, *Phys. Rev. A* **87**, 063623 (2013).
  - <sup>23</sup> Shang-Shun Zhang, Jinwu Ye and Wu-Ming Liu, *arXiv:1403.7031*.
  - <sup>24</sup> M. Aidelsburger, *et.al*, *Phys. Rev. Lett.* **107**, 255301 (2011). J. Struck, *et.al*, *Science* **333**, 996 (2011); *Phys. Rev. Lett.* **108**, 225304 (2012); *Nat. Phys.*, doi: 10.1038/nphys2750 (2013).
  - <sup>25</sup> M. Aidelsburger, *et.al*, *Phys. Rev. Lett.* **111**, 185301 (2013); H. Miyake, G. A. Siviloglou, C. J. Kennedy, W. C. Burton and W. Ketterle, *Phys. Rev. Lett.* **111**, 185302 (2013); C. J. Kennedy, G. A. Siviloglou, H. Miyake, W. C. Burton and W. Ketterle, *Phys. Rev. Lett.* **111**, 225301 (2013).
  - <sup>26</sup> Fa-Di Sun, Xiao-Lu Yu, Jinwu Ye, Heng Fan, W. M. Liu, *Scientific Reports* **3**, 2119 (2013).
  - <sup>27</sup> Fa-Di Sun, Jinwu Ye and W. M. Liu, Preprint.
  - <sup>28</sup> P. G. De Gennes, *Superconductivity of Metals and Alloys*, Perseus Books Publishing, L.L.C. 1999. In Page 96, the Eqn.14 was evaluated with respect to two-electrons wavefunction outside a Fermi surface which is the original Cooper-pair problem. Due to the absence of the Fermi surface, this two-body bound state discussed in<sup>14</sup> still differs from the original Cooper-pair problem.
  - <sup>29</sup> A.J. Leggett, *Quantum Liquids*, Oxford University Press, 2006.
  - <sup>30</sup> Immanuel Bloch, Jean Dalibard, Wilhelm Zwerger, *Rev. Mod. Phys.* **80**, 885 (2008).
  - <sup>31</sup> Jinwu Ye, *Phys. Rev. Lett.* **86**, 316 (2001); *Phys. Rev. Lett.* **87**, 227003 (2001); *Phys. Rev. B* **65**, 214505 (2002).
  - <sup>32</sup> Jinwu Ye, T. Shi and Longhua Jiang, *Phys. Rev. Lett.* **103**, 177401 (2009);
  - <sup>33</sup> T. Shi, Longhua Jiang and Jinwu Ye, *Phys. Rev. B* **81**, 235402 (2010)
  - <sup>34</sup> Jinwu Ye, Fadi Sun, Yi-Xiang Yu and Wuming Liu, *Ann. Phys.* **329** (2013), 51C72.

- <sup>35</sup> Jinwu Ye, J. Low Temp Phys. 158(5), 882-900 (2010). For a review, see : Yu Chen, Jinwu Ye and Quang Shan Tian, J. Low Temp Phys. 169 (2012), 149-168.
- <sup>36</sup> As shown in Sec.II-B, the reason to put a quotation mark on both “Cooper-pair wavefunction” and “Cooper-pair size” is that they are not really physical, so may not be really understood as the Cooper-pair wavefunction and Cooper-pair size. For the illustration purposes, they are evaluated here to compare with the physical pairing length and two-body bound state. Furthermore, several authors<sup>16,39</sup> also evaluated this un-physical length in different contexts. For notation simplicities, we dropped the quotation mark in the following.
- <sup>37</sup> J. R. Engelbrecht, M. Randeria, and C. A. R. Sá de Melo, Phys. Rev. B 55, 15153 (1997).
- <sup>38</sup> Christian H. Schunck, Yong-il Shin, Andr Schirotzek, Wolfgang Ketterle, Nature 454, 739-743 (7 August 2008).
- <sup>39</sup> N. Read and Dmitry Green, Phys. Rev. B 61, 10267C10297 (2000). For the purpose of making connections with the p-wave pairing nature of the non-abelian Pfaffian FQHE wavefunction, the “Cooper-pair wavefunction”  $g(\vec{r})$  is the suitable quantity to compare.
- <sup>40</sup> Note that  $\xi = \sqrt{\xi_x^2 + \xi_y^2 + \xi_z^2} = \frac{a_s}{\sqrt{2}}$  which is exactly the size of the two-body bound state in Eqn.32.
- <sup>41</sup> In Ref.<sup>16</sup>, only the  $l_i$  at the resonance  $\hbar/k_F a_s = 0$  was calculated. Our curve in Fig.4 at the resonance recovers their results. But as indicated in the text, the non-monotonic behaviors of  $l_i$  discovered in the Fig.4 can only be seen in the BCS side  $a_s < 0$ . Of course, as indicated in the text, the  $l_i$  can not be used to characterize the BCS to BEC crossover and is not an experimental measurable quantity anyway.
- <sup>42</sup> M. Randeria, J.-M. Duan, and L.-Y. Shieh, Phys. Rev. B 41, 327 (1990).
- <sup>43</sup> V. M. Loktev, R. M. Quick, and S. G. Sharapov, Phys. Rep. 349, 1 (2001).
- <sup>44</sup> Jinwu Ye and C. L. Zhang, Phys. Rev. A 84, 023840 (2011).
- <sup>45</sup> Yu Yi-Xiang, Jinwu Ye and W.M. Liu, Scientific Reports 3, 3476 (2013).
- <sup>46</sup> Masatoshi Sato, Yoshiro Takahashi and Satoshi Fujimoto, PRL 103, 020401 (2009)
- <sup>47</sup> Ming Gong, Sumanta Tewari, and Chuanwei Zhang, Phys. Rev. Lett. 107, 195303 (2011).
- <sup>48</sup> Xuebing Luo, K. Zhou, W. Liu, Z. Liang and Z. Zhang, Phys. Rev. A 89, 043612 (2014).